Murdoch
UNIVERSITY

Minakshi, M. (2010) *Lithium intercalation into amorphous FePO4 cathode in aqueous solutions.* Electrochimica Acta, 55 (28). pp. 9174-9178.

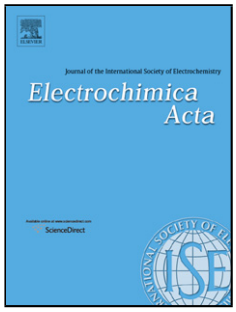

Title: Lithium Intercalation into Amorphous $FePO_4$ Cathode in Aqueous Solutions

Author: Manickam Minakshi

PII: S0013-4686(10)01170-9
DOI: doi:10.1016/j.electacta.2010.09.011
Reference: EA 16153

To appear in: *Electrochimica Acta*

Received date: 28-7-2010
Revised date: 5-9-2010
Accepted date: 5-9-2010

Please cite this article as: M. Minakshi, Lithium Intercalation into Amorphous $FePO_4$ Cathode in Aqueous Solutions, *Electrochimica Acta* (2010), doi:10.1016/j.electacta.2010.09.011

Lithium Intercalation into Amorphous $FePO_4$ Cathode in Aqueous Solutions

Manickam Minakshi
Faculty of Minerals and Energy, Murdoch University, Murdoch, WA 6150, Australia

Abstract

Amorphous iron phosphate ($FePO_4$) was investigated as a cathode material for battery applications using aqueous (lithium hydroxide or potassium hydroxide) electrolytes. Phosphate-based cathode materials are of great interest in lithium batteries which use non-aqueous electrolytes. In order for these materials to be used as cathodes in aqueous electrolytes it is important to understand their reduction/oxidation mechanisms. Potentiostatic and galvanostatic techniques are used to study these mechanisms. X-ray diffraction (XRD), Scanning electron microscopy (SEM) and X-ray photoelectron spectroscopy (XPS) have been used to gain insight into the reduction/oxidation behavior of $FePO_4$ cathodes. Our results show that $FePO_4$ undergoes reversible $Fe^{3+}/^{2+}$ processes of reduction and oxidation in LiOH electrolyte, while using KOH electrolyte this process is found to be irreversible. The lithium intercalation mechanism is identified for LiOH while in the case of KOH electrolyte H reacts to form FeOOH. The Zn|LiOH|$FePO_4$ battery provides a reversible capacity of 65 mAh/g. The results indicate the trigonal $FePO_4$ as an attractive host intercalation compound.

Keywords: Iron phosphate, rechargeable, battery, aqueous, trigonal.

* Corresponding author
Tel.: +61-8-9360-6784. Fax: +61-8-9310-1711. E-mail: minakshi@murdoch.edu.au; lithiumbattery@hotmail.com

1. Introduction

The cathode material of a rechargeable battery is a host insertion compound into/from which any alkali cations can be reversibly inserted/extracted over a compositional range during redox reactions [1]. The possible cathode materials providing good rechargeability are layered $LiCoO_2$, $LiNiO_2$ and spinel $LiMn_2O_4$. The use of $LiMn_2O_4$ alleviates the problems associated with Co and Ni toxicity and its cost, but the major issue hindering the development of this material is the loss of capacity with extensive cycling, particularly at elevated temperatures [2].

Following the oxide-based materials, a technological breakthrough occurred with the use of phosphates as cathodes in rechargeable non-aqueous lithium batteries. The cathode performance of a lithium iron phosphate ($LiFePO_4$) adopting an ordered olivine structure was first reported by Padhi et al. [3] who proposed $LiFePO_4$ as a potential cathode in non-aqueous batteries. Subsequently, extensive work on this material has been carried out by a number of researchers [4–8] and $LiFePO_4$ is now recognised as the active cathode for a new generation of lithium batteries. This is due to its low cost, environmentally-friendly properties and good rechargeability. The trigonal iron phosphate (analog of olivine) consists of corner shared framework with the FeO_4 and PO_4 tetrahedra. The only difference between trigonal and olivine structure is that of FeO_4 tetrahedra instead of the FeO_6 octahedra share common corners. $FePO_4$ has a potential application for an intercalation host compound [9].

The mechanism through which $LiFePO_4$ undergoes reduction/oxidation reactions in non-aqueous lithium battery has been widely discussed in the literature [10–13]. The focus of this paper is to investigate $FePO_4$ for use with aqueous electrolytes. The current work follows our extensive research on MnO_2 [14] in aqueous solution where we reported that the reduction mechanism involves both

lithium (Li^+) and proton (H^+) intercalation, but protons cannot de-intercalate reversibly. However, incorporation of additives [15–16] into MnO_2 leads to improved electrochemical performance while preventing the formation of non-rechargeable products. This has motivated the search for new cathode materials suitable for aqueous rechargeable batteries.

Here, we report on the electrochemical performance of trigonal $FePO_4$ as a cathode material in a rechargeable cell based on LiOH or KOH electrolytes. Zn metal is chosen as anode material. The use of trigonal $FePO_4$ in a non-aqueous lithium battery was reported by Okada et al. [17] whereas its application in a cell with aqueous LiOH and KOH solution is reported here for the first time.

2. Experimental

2.1 Synthesis

The amorphous iron phosphate ($FePO_4$) material used in this work was synthesized by a simple and inexpensive method identical to that described by Okada et al. [17]. The stoichiometric ratios of starting materials such as metallic iron and P_2O_5 were mixed in ethanol for an hour in an agate mortar. The slurry was evaporated at 90 °C for 30 min and the resultant precursor was fine ground and calcined at 200 °C for 12 h to yield the amorphous $FePO_4$ material. The $Fe^{3+}/^{2+}$ redox couple in the amorphous iron phosphate is reported [17] to be fully reversible than the crystalline counterpart. The crystalline $FePO_4$ phase is known to be electrochemically inactive [18]. Hence, in this work, synthesis temperature is chosen to be 200 °C.

2.2 Material Characterization

The products formed during the cathodic and anodic scan were characterized by X-ray diffraction (XRD), X-ray photoelectron spectroscopy (XPS) and Scanning electron microscopy (SEM). For XRD analysis, X-ray diffractometer (Siemens) using Cu-Kα

radiation was used. XPS (Kratos Ultra Axis Spectrometer) using monochromatic Al Kα (1486.6 eV) radiation was used to analyze the chemical binding energies of the samples. XPS analysis was started when the pressure in the analysis chamber fell below 1 x 10^{-9} hPa. Carbon, C (1s), was used as a reference for all samples. A SEM (Philips Analytical XL series 20) was used for surface analysis investigations.

2.3 Potentiostatic measurements: Slow-scan cyclic voltammetry

For cyclic voltammetry (CV) experiments, a three-electrode cell was used. The working electrode was disk-shaped (10 mm diameter with 1 mm thickness) $FePO_4$. This disk was embedded in Pt gauze through which the electrical contact was made. On the other side of the disk, a layer of carbon was also pressed. The disk was inserted in a Teflon barrel on top of the carbon side and electrical contact was made by means of a brass plunger. The working $FePO_4$ surface was exposed to electrolyte through a hole of 1 mm in the Teflon barrel. The counter-electrode was strip of Zn foil, separated from the main electrolyte by means of a porous frit. Hg/HgO served as the reference electrode. The electrolyte was a 5 M of either lithium hydroxide or potassium hydroxide. The working electrode was cycled between 0.2 to –0.4 V at 25 μV /s scan rate. On each occasion, the potential scan started at 0.2 V, moving initially in the cathodic direction. At the reduction and oxidation points of the experiment, the cathode material was removed from the solution, washed with water and characterized by XRD, XPS and SEM analysis. All the cyclic voltammetry experiments were done using an EG & G Princeton Applied Research Versa Stat III model. All potentials were measured relative to the Hg/HgO electrode. All the electrochemical measurements were carried out in an ambient room atmosphere (25 ± 1^{o} C).

2.4 Galvanostatic discharge/charge of Zn|LiOH|$FePO_4$ cell

The $FePO_4$ active material was first mixed with 15 wt. % of carbon black (A-99, Asbury USA) and with 10 wt. % of poly(vinylidene difluoride) (PVDF, Sigma Aldrich) as a binder and then pressed into a disk shape with a diameter of 10 mm. Each disk was 0.5 mm thick and weighed approximately 35 mg. An electrochemical test cell was constructed with the disk as cathode, Zn metal as anode and filter paper (Whatman filters 12) as separator. The mass of zinc was at least ten times greater (to overcome the Zn depletion) than that required for a stoichiometric reaction between Zn and $FePO_4$. The electrolyte was a 5 M of lithium hydroxide. Analytical reagent grade lithium hydroxide monohydrate ($LiOH{\bullet}H_2O$) and potassium hydroxide (KOH) were dissolved in de-ionized water to prepare solutions of the required concentrations. The cell was discharged/charged galvanostatically at 0.5 mA/cm^2 by using an 8 channel battery analyser from MTI Corporation, USA, operated by a battery testing system (BTS).

3. Results and Discussion

3.1 Slow scan cyclic voltammetric investigation of $FePO_4$

To study the reduction/oxidation mechanism of an $FePO_4$ cathode, slow scan cyclic voltammetry (CV) was used. In the CV technique, the potential determines the electrochemical reaction that occurs. The study involved slow scan CV in conjunction with the characterization of the materials formed during the electrochemical reduction and oxidation of $FePO_4$ by using various techniques i.e. XRD, SEM and XPS.

The first and tenth cyclic voltammogram of $FePO_4$ in a LiOH aqueous electrolyte using Hg/HgO reference electrode is displayed in Fig. 1. The potential is displayed on the x-axis with potentials becoming more negative from right to left. A negative-going potential generates more strongly reducing conditions while a positive-going potential becomes more strongly oxidising. Current is shown on the y-

axis. A negative current corresponds to a reduction from Fe^{3+} to Fe^{2+} while a positive current is due to oxidation of Fe^{2+} to Fe^{3+}. At the potential where current is maximum is defined as a peak. The voltammogram consists of a reduction peak C_1 at -275 mV and a corresponding anodic peak A_1 at -12 mV. Figure 1 also shows the changes in CV profile when the material is subjected to continuous cycling (10 cycles) in the same potential region. In the tenth cycle, the cathodic and anodic peak current decreased to 85% and 10% (reducing the efficiency by 15% and 10%) respectively, however the material could be reversibly reduced/oxidised over multiple cycles. The observed reduction and oxidation potentials at -275 and -12 mV are less negative and positive than the hydrogen and oxygen evolution potentials that occur, suggesting that $FePO_4$ can be used as a cathode material in aqueous LiOH electrolyte.

In accordance with the objective of this work, the effect of replacing KOH with LiOH was determined by carrying out a cyclic voltammogram on two identical cells, one containing LiOH and the other KOH electrolyte. The behavior of $FePO_4$ in aqueous LiOH cell can be compared to that in aqueous KOH by referring to Fig. 2. The CVs of $FePO_4$ in the two electrolytes appear to be quite different. Two reduction peaks (C_1 and C_2) and an oxidation peaks (A_1) are seen for the cell using KOH electrolyte, in the LiOH cell only one reduction (C_1) and one oxidation peak (A_1) are seen. Upon continuous cycling (in Fig. 3) in the same potential region as for KOH cell, the cathodic peak C_1 disappears and the shape of the peak C_2 is changed. The anodic peak A_1 becomes more pronounced on cycling.

The redox potential observed for the LiOH cell is almost the same as values reported in the literature [10–13] for the non-aqueous electrolyte. Hence, this could correspond to a lithium intercalation/de-intercalation mechanism associated with the $Fe^{3+}/^{2+}$ redox couple. While for the KOH cell, during an initial cycle, K^+ ion insertion

is observed [19] as peak C_1, but this process is not reversible after the 5th cycle in Fig. 3. The size of the K^+ ion (1.38 Å) is twice that of Li^+ (0.76 Å) in a VI-fold coordination [20] and hence the host trigonal structure is not stable for insertion/extraction of K^+ ions. Hence the cathodic peak C_1 corresponding to K^+ intercalation disappeared upon successive cycles. The peak C_2 corresponds to well-known proton insertion [21-22] into $FePO_4$ in aqueous KOH electrolyte which is reversible. Hence, unlike for Li^+, the intercalation mechanism of K^+ is not reversible in the $FePO_4$ structure.

3.2 Characterization of the $FePO_4$ cathode material

The change in crystal structure after electro-reduction and electro-oxidation has been studied for the $FePO_4$ cathode by X-ray diffraction measurements as shown in Fig. 4. The XRD pattern of the starting material (Fig. 4a) show that it is poorly crystalline and the tiny peaks are assigned to trigonal $FePO_4$ [23]. Figs. 4b and 4c show the XRD patterns of the material formed on scanning $FePO_4$ to C_1 (-275 mV) and A_1 (-12 mV) where reduction and oxidation occurs. The generation of new peaks in Fig. 4b match those reported in the literature [10, 24] and is in agreement with the simulated pattern shown (Fig. 4c) for lithium intercalated iron phosphate ($LiFePO_4$), which indicates that $LiFePO_4$ is formed by the reduction of $FePO_4$. This new material adopts an olivine structure of orthorhombic system [25] with intercalated lithium and iron cations located in octahedral sites. Thus the electro-reduction of $FePO_4$ in aqueous LiOH electrolyte involves the intercalation of Li^+ and hence the mechanism is quite similar to that reported in non-aqueous electrolyte. After the subsequent electro-oxidation, material formed in the oxidation cycle regenerates the original material. The XRD pattern (Fig. 4d) of the regenerated material is almost identical to that of the original $FePO_4$ (in Fig. 4a) except for peaks at 2θ = 35.3 and 57 indicating the

presence of $LiFePO_4$ material. The differences observed in the crystal structure from the delithiated phase of $LiFePO_4$ and trigonal $FePO_4$ are given in the literature [17].

The XRD pattern of the $FePO_4$ material formed after electro-reduction at -335 mV and electro-oxidation at -14 mV in the KOH electrolyte is compared with the starting material in Fig. 5. The mechanism by which $FePO_4$ reduces is different from that of LiOH electrolyte. As can be seen from Fig. 5b, an evolution of new peaks is observed in the reduced material in addition to the parent compound. Clearly, these new peaks do not correspond to any of the lithium intercalated $FePO_4$. However, these peaks are associated with the formation of the FeOOH (goethite) structure [26]. This suggests that the reduction mechanism of the $FePO_4$ cathode material is not the same as that observed for LiOH electrolyte. The XRD pattern (Fig. 5c) of the electro-oxidised material reverted back to the original material in addition to the formation of Fe_2O_3 which is found to be not reversible.

The surface morphologies of the $FePO_4$ cathode material formed after electro-reduction and electro-oxidation in LiOH and KOH electrolytes were determined by scanning electron microscopy. As can be seen from the micrograph, Fig. 6a, the morphology appears to be poorly crystalline as observed in the XRD spectra. The material formed after electro-reduction had a different morphology (Fig. 6b). A crystalline-like material of particle size 5-10 μm is observed, this could be a new phase ($LiFePO_4$) generated by reduction. The subsequent oxidation of the reduced material (Fig. 6c) produced a phase ($FePO_4$) whose morphology was quite similar to that of the original material. This was in contrast with the material (Fig. 7) formed after electro-reduction and oxidation of $FePO_4$ in the KOH cell. As evidenced by the XRD patterns (Fig. 5b-c), the observed morphology could be due to the formation of

iron oxy-hydroxide (FeOOH) during reduction and iron (III) oxide (Fe_2O_3) during subsequent oxidation that underwent an irreversible change during the cycle.

To confirm the presence of lithium ions in the electro-reduced/oxidised trigonal $FePO_4$ structure, an XPS analysis was carried out. Fig. 8 shows the XPS spectra of Li (1s) for the $FePO_4$ cathode. The material after electrochemical processes was found to be covered with a layer of Li_2CO_3 been formed through the reaction of LiOH by the atmospheric CO_2. This is not unexpected because the atmospheric CO_2 is not excluded from the experiment as the cell is not completely sealed. Hence, the material was washed thoroughly with acetone and de-ionised water several times until no further Li^+ ions were detected as indicated by the colour of the washings in the presence of phenolphthalein indicator. The washed material was mounted in the XPS analysis chamber and the spectra were recorded. It can be seen that the peak at 55.7 eV, corresponding to Li, has a high intensity for electro-reduced but very low intensity for electro-oxidised sample. This low in intensity peak confirms that a small amount of lithium associated with $FePO_4$ is still present even after oxidation, as what seen in the XRD pattern of Fig. 4d. From the evidence of XRD and XPS studies, it can be concluded that lithium is intercalated into the host $FePO_4$ when aqueous LiOH is the electrolyte. The mechanism is found to be reversible.

3.3.Galvanostatic discharge-charge of FePO4 in LiOH electrolyte

The Zn|LiOH|$FePO_4$ cell was discharged and charged galvanostatically at 0.5 mA/cm^2 using a battery analyser. A typical discharge-charge curve of the aqueous cell is shown in Fig. 9. The initial open-circuit voltage was around 1.0 V. On discharge, the cell voltage fell at a constant rate to 0.4 V corresponding to 60 mAh/g and then decreased sharply to a cut-off voltage of 0.2 V. The overall discharge capacity is calculated to be 65 mAh/g. Upon charging the material at constant current, the voltage

increased steeply to 1.4 V corresponding to 40 mAh/g and then the voltage gradually increased to a cut-off voltage of 1.6 V. The charge capacity is fully reversible, as reflected in the cyclic voltammetry (Fig. 1) experiment that the $Fe^{3+}/^{2+}$redox couple is fully accessible for amorphous $FePO_4$ material. Thus, within the operating voltage window maximum capacity was derived from the $FePO_4$ material. The cycleability of the $FePO_4$ battery has been examined and it was found that cycleability retention wasn't very attractive to be suitable for energy storage applications. This could be due to the formation non-rechargeable products which are inevitable in aqueous solutions. However, these products could be suppressed by adding suitable additives [15-16] to the $FePO_4$ cathode to enhance the performance. Trigonal $FePO_4$ might be a potential cathode material for an aqueous battery system provided its stability in alkaline electrolyte and electrochemical properties are improved.

4. Conclusions

Lithium intercalation into a $FePO_4$ cathode in an aqueous electrolyte has been investigated. Cyclic voltammetry results show that $FePO_4$ undergoes a reversible (Fe^{3+}/Fe^{2+}) process of reduction and oxidation in lithium hydroxide electrolyte. X-ray diffraction of the reduced and oxidised $FePO_4$ shows that the process undergoes a lithium intercalation and de-intercalation mechanism to form $LiFePO_4$ and $FePO_4$. An X-ray photoelectron spectroscopy study confirms the presence of lithium in the solid matrix of the $FePO_4$ cathode. Whereas, using KOH electrolyte, intercalation of the potassium ion (K^+) is associated with proton intercalation during reduction. K^+ ion intercalation is found to be irreversible in the successive cycles. The discharge capacity of the Zn|LiOH|$FePO_4$ battery was calculated to be 65 mAh/g. The discharge voltage of this battery needs to be improved to compete with well-established non-aqueous counterparts. Nevertheless, this material is an interesting alternative for

lithium intercalation in terms of low cost, environmental friendliness and safety issues.

Acknowledgement

The author wishes to acknowledge the Australian Research Council (ARC). This article was produced as an outcome of the ARC Discovery Project grant (DP1092543).

References

[1] M. S. Whittingham, Chem. Rev. **104** (2004) 4271.

[2] Y. Shin and A. Manthiram, Electrochem. Solid State Lett. **5(3)** (2002) A55.

[3] A. K. Padhi, K.S. Nanjundaswamy, C. Masquelier, S. Okada and J. B. Goodenough, J. Electrochem. Soc. **144** (1997) 1609.

[4] K. Konstantinov, S. Bewlay, G. X. Wang, M. Lindsay, J.Z. Wang, H.K. Liu, S.X. Dou and J.-H. Ahn, Electrochim. Acta **50** (2004) 421.

[5] C. H. Mi, G.S. Cao and X.B. Zhao, Mater. Lett. **59** (2005) 127.

[6] B. Wang, Y. Qiu and S. Ni, Solid State Ionics **178** (2007) 843.

[7] F. Yu, J. Zhang, Y. Yang and G. Song, Electrochim. Acta **54** (2009) 7389.

[8] X. Gao, G. Hu, Z. Peng and K. Du, Electrochim. Acta **54** (2009) 4777.

[9] H. Okawa, J. Yabuki, Y. Kawamura, I. Arise and M. Sato, Mat. Res. Bull. **43** (2008) 1203.

[10] A.K. Padhi, K.S. Nanjundaswamy and J. B. Goodenough, J. Electrochem. Soc. 144 (1997) 1188.

[11] C.V. Ramana, A. Mauger, F. Gendron, C. M. Julien and K. Zaghib, J. Power Sources **187** (2009) 555.

[12] N. Kalaiselvi and A. Manthiram, J. Power Sources **195** (2010) 2894.

[13] J. Molenda, W. Ojczyk, K. Swierczek, W. Zajac, F. Krok, J. Dygas and R. Liu, Solid State Ionics **177** (2006) 2617.

[14] M. Minakshi, P. Singh, T.B. Issa, S. Thurgate and R. DeMarco, J. Power Sources **130** (2004) 254.

[15] M. Minakshi and D. R. G. Mitchell, Electrochim. Acta **53** (2008) 6323.

[16] M. Minakshi, D. R. G. Mitchell and P. Singh, Electrochim. Acta **52** (2007) 3294.

[17] S. Okada, T. Yamamoto, Y. Okazaki, J. Yamaki, M. Tokunaga and T. Nishida, J. Power Sources **146** (2005) 570.

[18] Y. Song, S. Yang, P.Y. Zavalij and M.S. Whittingham, Mat. Res. Bull. **37** (2002) 1249.

[19] M. Minakshi, J. Electroanal. Chem. **616** (2008) 99.

[20] R.D. Shannon, Acta. Crystallogr. **A 32** (1976) 751.

[21] H. Schlorb, M. Bungs and W. Plieth, Electrochim. Acta **42** (1996) 2619.

[22] K. S. Abou-El-Sherbini and M. H. Askar, J. Solid State Electrochem. **7** (2003) 435.

[23] International Centre for Diffraction Data No. 29-0715.

[24] M. Minakshi, P. Singh, T. B. Issa, S. Thurgate, and K. Prince, Key Engineering Materials, **320** (2006) 271.

[25] K. F. Hsu, S. K. Hu, C. H. Chen, M. Y. Cheng, S. Y. Tsay, T. C. Chou, H. S. Sheu, J. F. Lee and B. J. Hwang, J. Power Sources **192** (2009) 660.

[26] International Centre for Diffraction Data No. 44-1415.

Figure Captions

Fig. 1 A typical cyclic voltammogram of iron phosphate ($FePO_4$) in aqueous lithium hydroxide electrolyte (scan rate: 25 μV. s^{-1}; potential limit: 0.2 to -0.4 V and back). Cycle numbers are indicated in the figure.

Fig. 2 Cyclic voltammogram of $FePO_4$ in aqueous lithium hydroxide and potassium hydroxide electrolytes for the first cycle. The potential scanned at 25 μV. s^{-1} from 0.2 to -0.4 V and back.

Fig. 3 Cyclic voltammogram of $FePO_4$ in aqueous potassium hydroxide electrolyte for the repeated cycles, potential scanned at 25 μV. s^{-1} from 0.2 to -0.4 V and back. The numbers in figures denoted cycle number.

Fig. 4 X-ray diffraction patterns of $FePO_4$ (a) before electro reduction (b) after the first cycle of electro reduction at -275 mV (c) simulated pattern of $LiFePO_4$: orthorhombic – olivine like structure (PNMA space group) and (d) after subsequent electro oxidation at -12 mV in aqueous LiOH electrolyte.

Fig. 5 X-ray diffraction patterns of $FePO_4$ (a) before electro reduction (b) after the first cycle of electro reduction at -335 mV and (c) after subsequent electro oxidation at -14 mV in aqueous KOH electrolyte.

Fig. 6 Scanning electron images of $FePO_4$ (a) before electro reduction (b) after the first cycle of electro reduction and (c) after subsequent electro oxidation in aqueous LiOH electrolyte.

Fig. 7 Scanning electron images of $FePO_4$ (a) after the first cycle of electro reduction and (b) after subsequent electro oxidation in aqueous KOH electrolyte.

Fig. 8 XPS spectra of Li 1s of $FePO_4$ (a) after the first cycle of electro reduction and (b) after subsequent electro oxidation in aqueous LiOH electrolyte.

Fig. 9 First (Galvanostatic) discharge-charge cycle of Zn-$FePO_4$ cell using aqueous LiOH electrolyte.

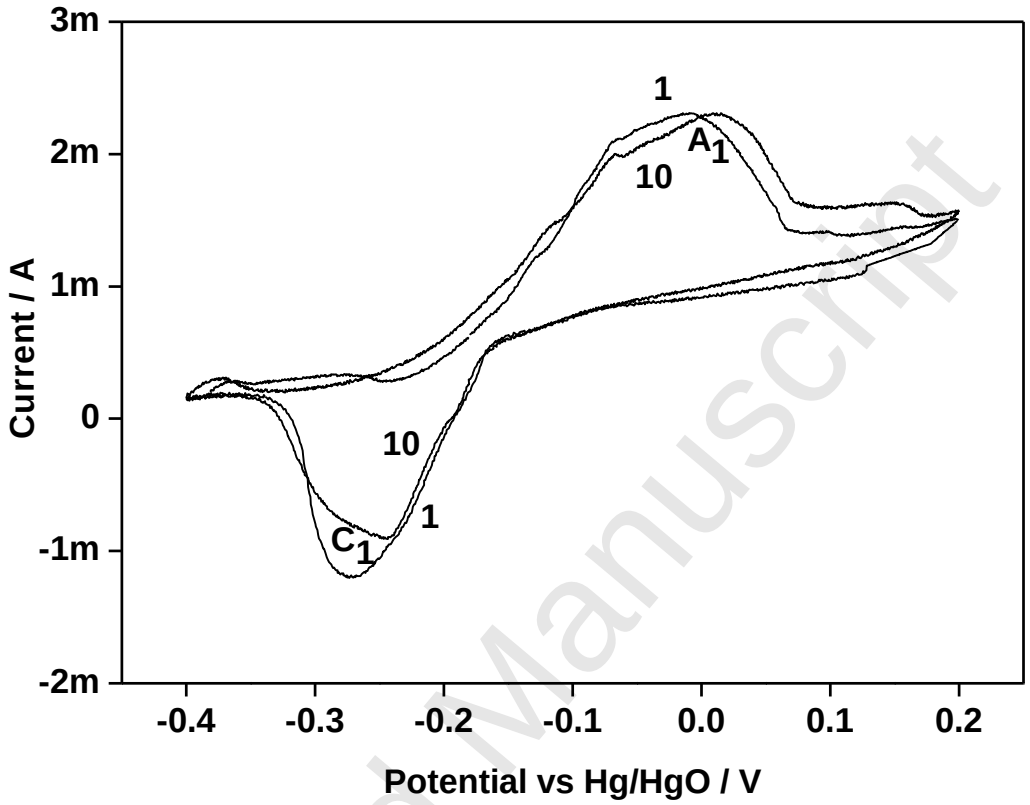

Fig. 1 A typical cyclic voltammogram of iron phosphate ($FePO_4$) in aqueous lithium hydroxide electrolyte (scan rate: 25 µV. s^{-1}; potential limit: 0.2 to -0.4 V and back). Cycle numbers are indicated in the figure.

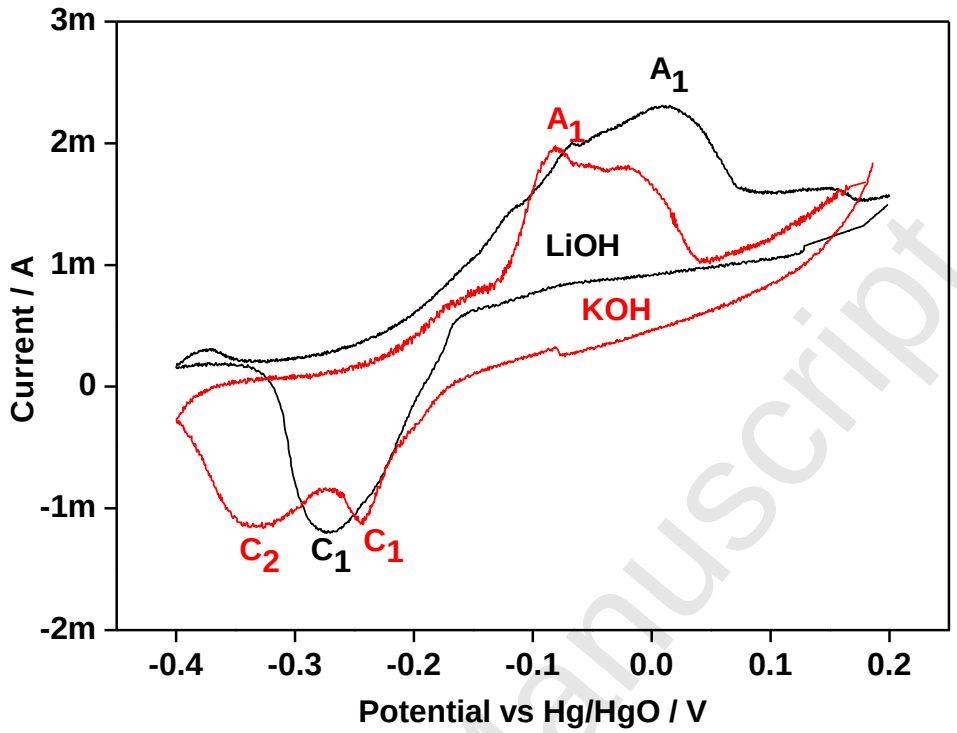

Fig. 2 Cyclic voltammogram of $FePO_4$ in aqueous lithium hydroxide and potassium hydroxide electrolytes for the first cycle. The potential scanned at 25 µV. s^{-1} from 0.2 to -0.4 V and back.

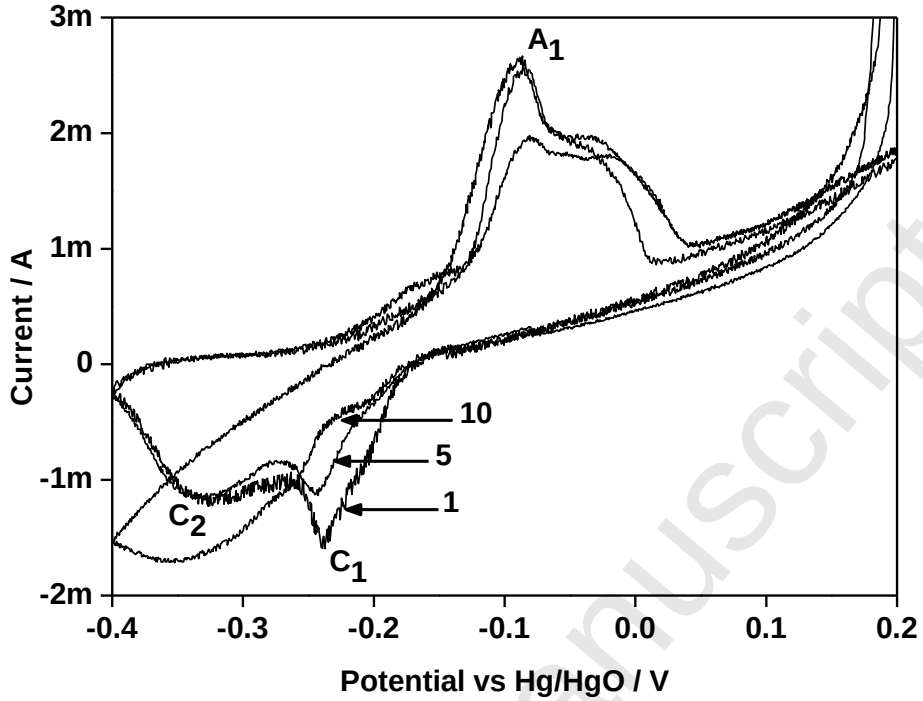

Fig. 3 Cyclic voltammogram of $FePO_4$ in aqueous potassium hydroxide electrolyte for the repeated cycles, potential scanned at 25 µV. s^{-1} from 0.2 to -0.4 V and back. The numbers in figures denoted cycle number.

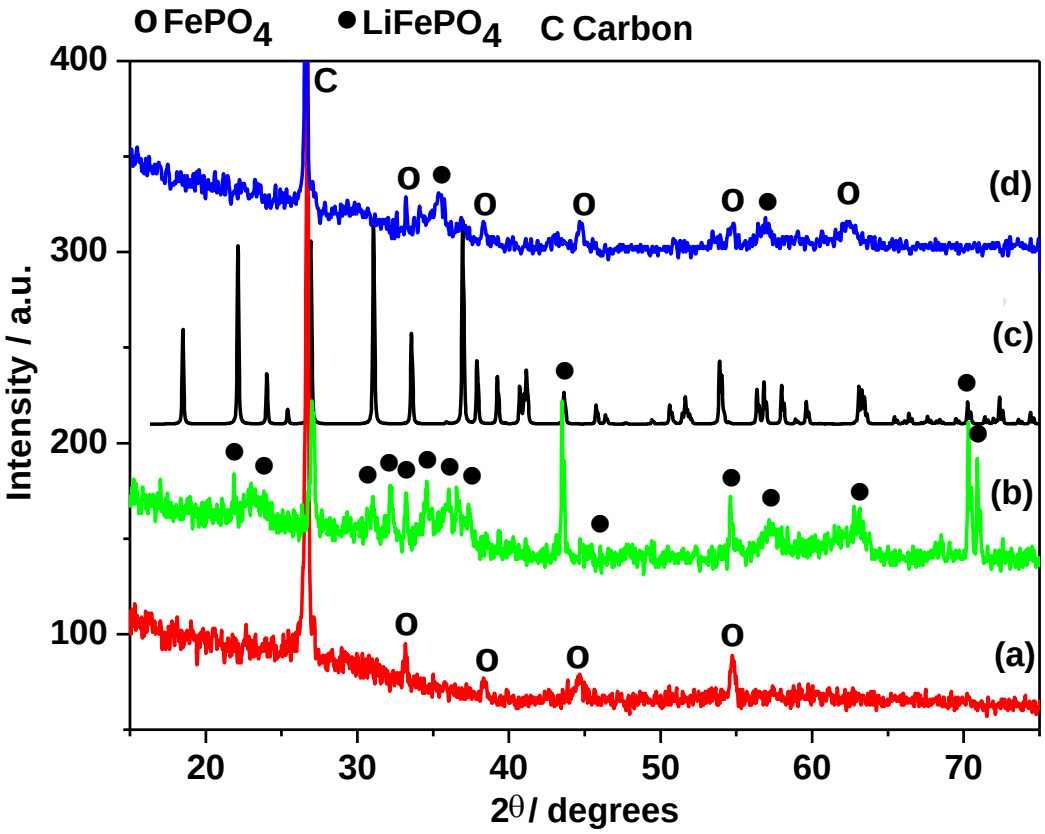

Fig. 4 X-ray diffraction patterns of $FePO_4$ (a) before electro reduction (b) after the first cycle of electro reduction at -275 mV (c) simulated pattern of $LiFePO_4$: orthorhombic – olivine like structure (PNMA space group) and (d) after subsequent electro oxidation at -12 mV in aqueous LiOH electrolyte.

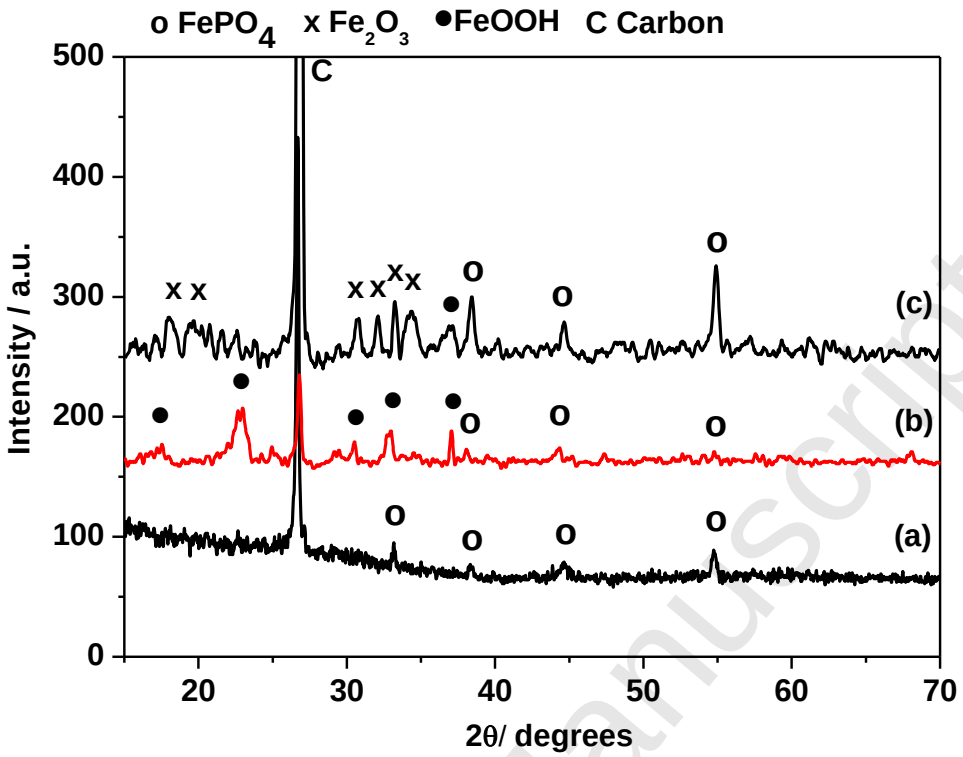

Fig. 5 X-ray diffraction patterns of $FePO_4$ (a) before electro reduction (b) after the first cycle of electro reduction at -335 mV and (c) after subsequent electro oxidation at -14 mV in aqueous KOH electrolyte.

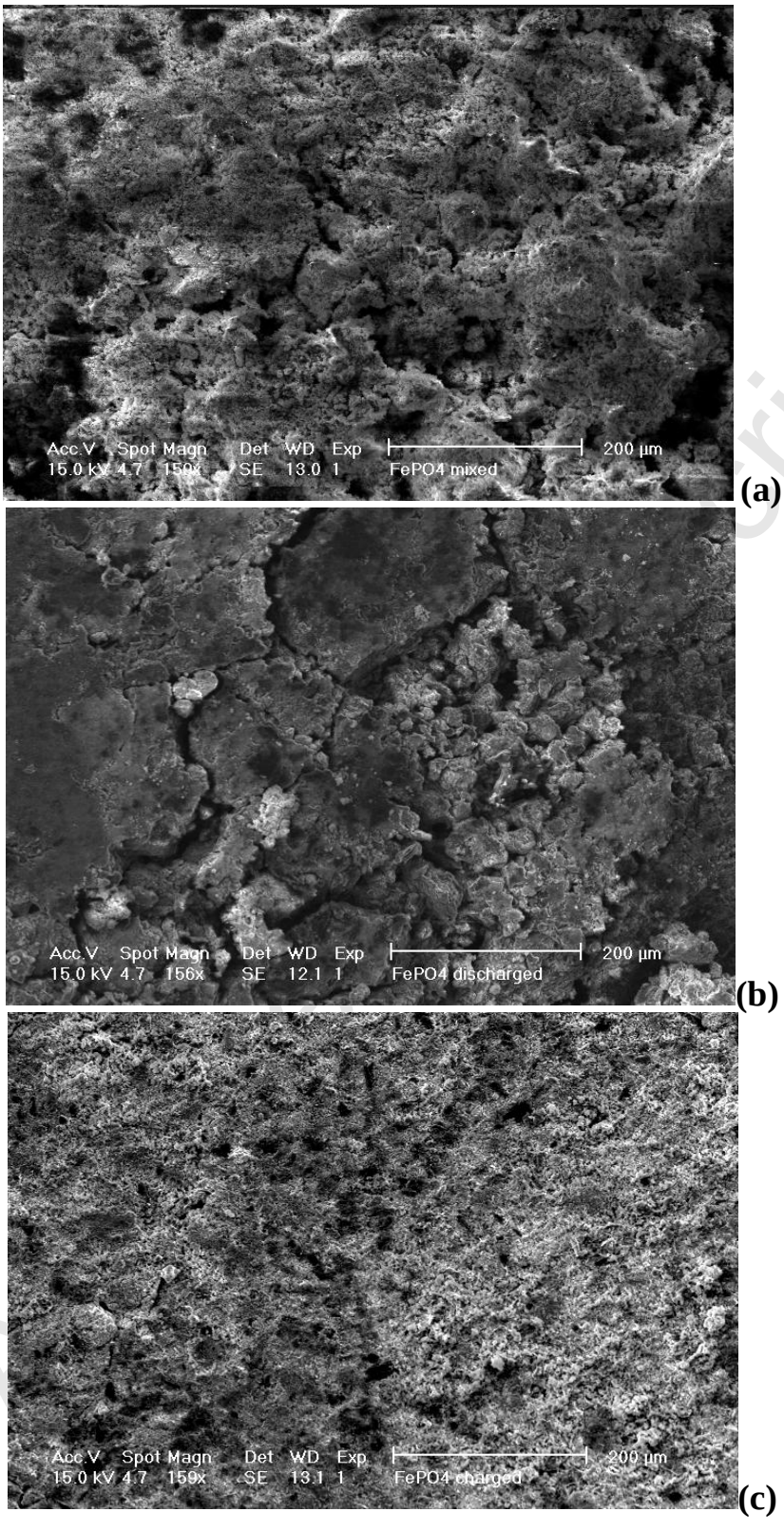

Fig. 6 Scanning electron images of $FePO_4$ (a) before electro reduction (b) after the first cycle of electro reduction and (c) after subsequent electro oxidation in aqueous LiOH electrolyte.

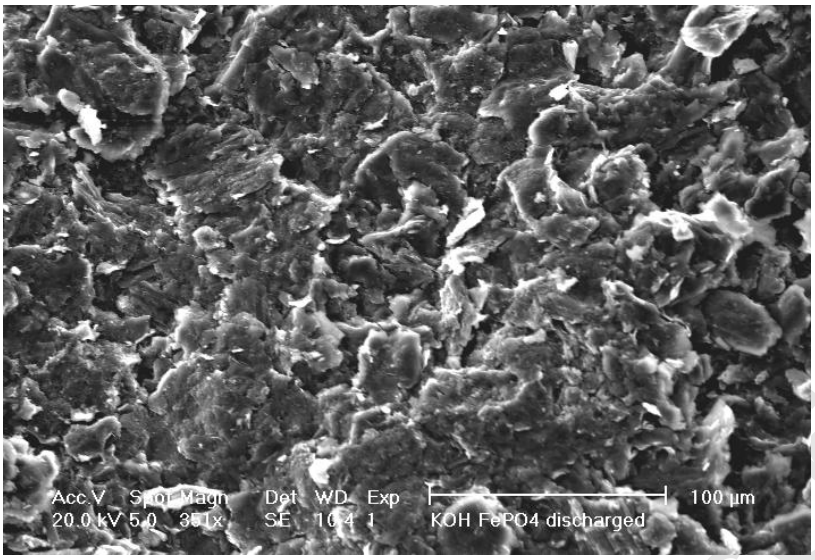

(a)

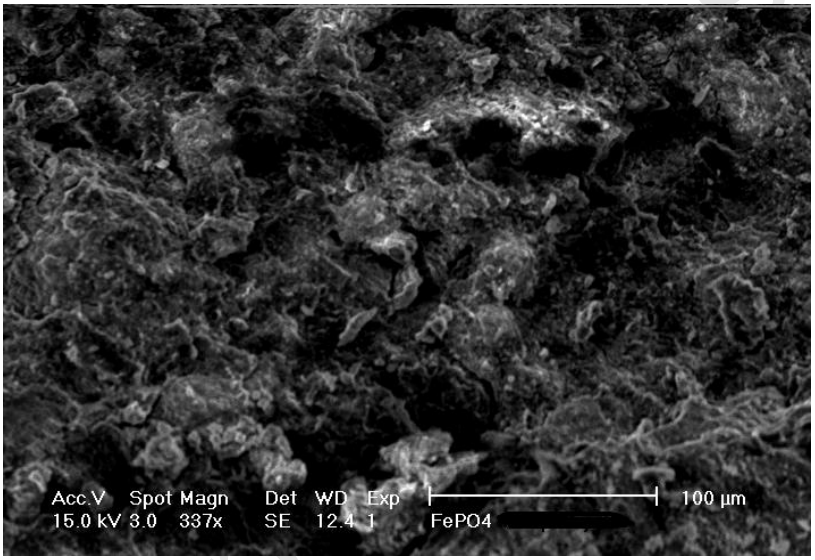

(b)

Fig. 7 Scanning electron images of $FePO_4$ (a) after the first cycle of electro reduction and (b) after subsequent electro oxidation in aqueous KOH electrolyte.

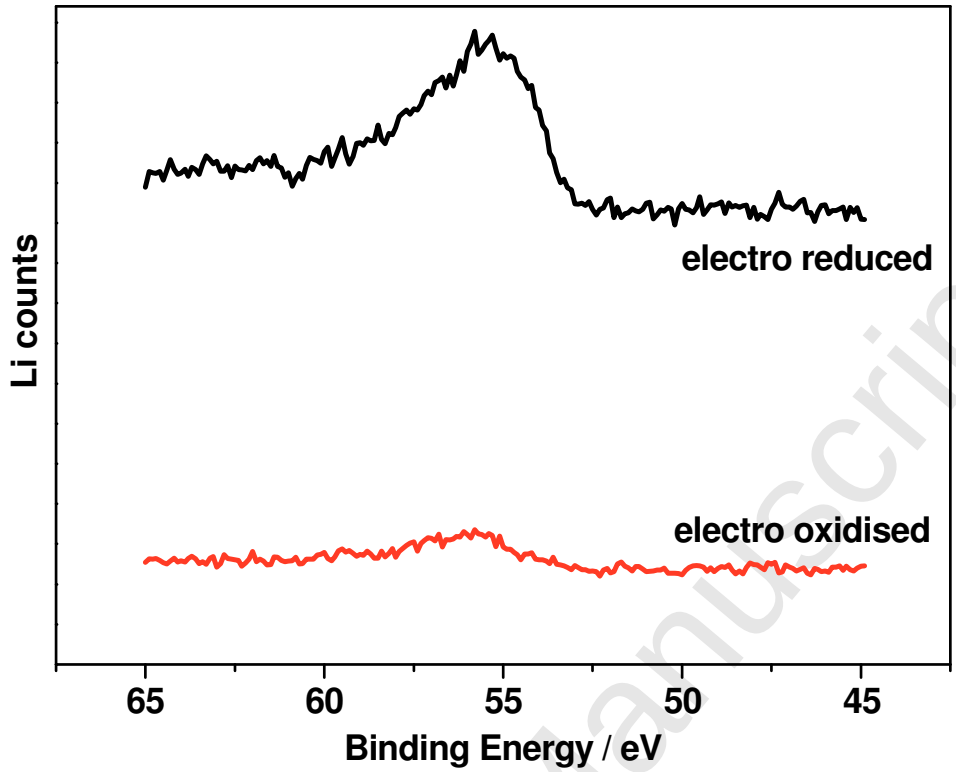

Fig. 8 XPS spectra of Li 1s of $FePO_4$ (a) after the first cycle of electro reduction and (b) after subsequent electro oxidation in aqueous LiOH electrolyte.

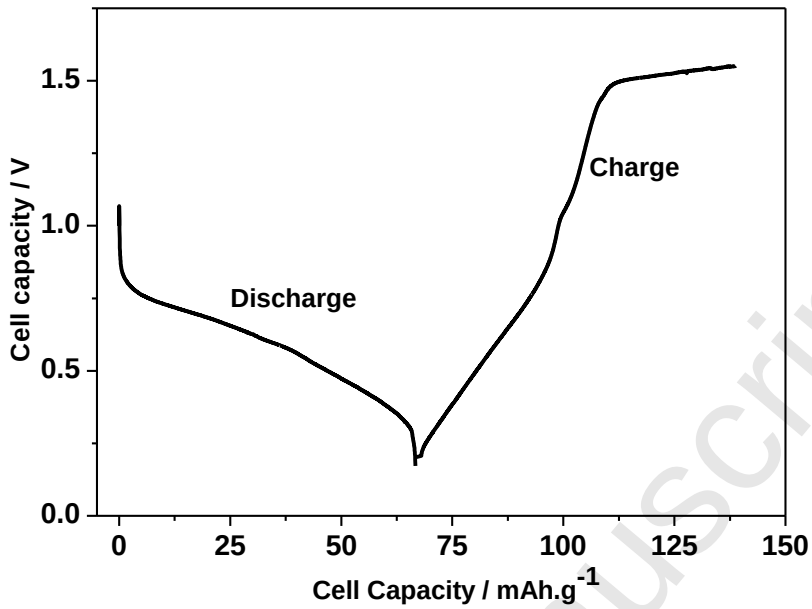

Fig. 9 First (Galvanostatic) discharge-charge cycle of Zn-$FePO_4$ cell using aqueous LiOH electrolyte.